Structure, Vol. 12, 1533–1544, August, 2004, ©2004 Elsevier Ltd. All rights reserved. DOI 10.1016/j.str.2004.05.024

The Crystal Structure of the RNA-Dependent RNA Polymerase from Human Rhinovirus: A Dual Function Target for Common Cold Antiviral Therapy

Robert A. Love,* Karen A. Maegley, Xiu Yu, Rose Ann Ferre, Laura K. Lingardo, Wade Diehl, Hans E. Parge, Peter S. Dragovich, and Shella A. Fuhrman
Pfizer Global Research and Development
La Jolla Laboratories
San Diego, California 92121

Summary

Human rhinoviruses (HRV), the predominant members of the *Picornaviridae* family of positive-strand RNA viruses, are the major causative agents of the common cold. Given the lack of effective treatments for rhinoviral infections, virally encoded proteins have become attractive therapeutic targets. The HRV genome encodes an RNA-dependent RNA polymerase (RdRp) denoted 3D^{pol}, which is responsible for replicating the viral genome and for synthesizing a protein primer used in the replication. Here the crystal structures for three viral serotypes (1B, 14, and 16) of HRV 3D^{pol} have been determined. The three structures are very similar to one another, and to the closely related poliovirus (PV) 3D^{pol} enzyme. Because the reported PV crystal structure shows significant disorder, HRV 3D^{pol} provides the first complete view of a picornaviral RdRp. The folding topology of HRV 3D^{pol} also resembles that of RdRps from hepatitis C virus (HCV) and rabbit hemorrhagic disease virus (RHDV) despite very low sequence homology.

Introduction

Picornaviruses are a large group of nonenveloped, positive-strand RNA viruses with a common genetic organization and replication strategy (Racaniello, 2001). This family includes the human rhinoviruses (HRV), the major causative agents of the common cold, and enteroviruses, as represented by poliovirus (PV). HRV and PV are very similar in genome organization (~7200 and 7500 nucleotides, respectively), polyprotein structure and processing, and viral protein function (Kitamura et al., 1981; Skern et al., 1985). Over 100 serotypes of rhinoviruses have been reported, and the majority recognize ICAM-1 as a cellular receptor (Greve et al., 1989) while the rest utilize the LDL receptor (Hofer et al., 1994). The complete genome sequence has been determined for only a few HRV serotypes: 14, 16, and 89 from the ICAM-1 class; and 1B and 2 from the LDL class.

Unlike poliovirus, the development of vaccines against rhinovirus is hindered by the large number of serotypes and weak cross-protection between serotypes. While most HRV infections are self-limiting, they can cause serious complications in persons with chronic respiratory disease or immunodeficiencies (Couch, 2001). For both healthy and high-risk individuals, antiviral treatment or prophylaxis would be desirable. However, no antiviral agents are currently approved for the prevention/treatment of HRV infection, although several have shown potent in vitro activity against HRV in cell culture, such as viral capsid binders (Gwaltney et al., 2002) and protease inhibitors (Patick et al., 1999).

After the binding of a picornavirus to its receptor and insertion of viral RNA into the cytoplasm, the parental RNA serves as mRNA to produce an initial polypeptide which then self cleaves to give enzymes and structural proteins (Racaniello, 2001). Among the best-studied picornaviral enzymes are two nonstructural proteins denoted 3C^{pro} and 3D^{pol}. 3C^{pro} is a cysteine protease responsible for most of the polyprotein cleavage and has been a focus of recent drug design efforts (Johnson et al., 2002). 3D^{pol}, encoded by the C-terminal portion of the viral polyprotein, is an RNA-dependent RNA polymerase (RdRp) which copies the viral genome through an intermediate negative strand prior to encapsidation into infectious progeny virions (Cameron et al., 2002). This replication occurs in a primer-dependent manner on membranous vesicles in the cytoplasm of the infected cell. 3D^{pol} also catalyzes the covalent linkage of UMP to a tyrosine on a short peptide encoded by 3B (denoted VPg), with uridylylated VPg then serving as a protein primer for the initiation of RNA replication (Paul et al., 1998). Therefore, HRV 3D^{pol} possesses two distinct enzymatic functions which could be targeted for inhibition.

Crystal structures have been determined for several viral RdRps, such as poliovirus 3D^{pol} (Hansen et al., 1997), hepatitis C virus (HCV) NS5B (Ago et al., 1999; Bressanelli et al., 1999; Lesburg et al., 1999), rabbit hemorrhagic disease virus (RHDV) polymerase (Ng et al., 2002), bovine viral diarrhea virus (BVDV) polymerase (Choi et al., 2004), and bacteriophage ϕ6 polymerase (Butcher et al., 2001). These structures display a common overall architecture found in all oligonucleotide polymerases and described as a right hand with thumb, fingers, and palm domains (Steitz, 1999). In addition, RdRps have the unique feature of bridging finger and thumb domains, giving a relatively closed and spherical appearance. In the structure of PV 3D^{pol}, much of the fingers domain is disordered; thus characterization of picornaviral RdRp architecture has remained incomplete. Here we report the crystal structures of HRV 3D^{pol} derived from three distinct serotypes: 1B from the minor LDL receptor class, and 16 and 14 from the major ICAM-1 receptor binding class. Each structure reveals a fully ordered enzyme with the same tertiary fold and clear similarity to other members of the RdRp family.

Results and Discussion

Structure Determination

The crystal structure of HRV14 3D^{pol} was solved by taking advantage of the strong binding of lanthinides at a magnesium site in the enzyme's catalytic center. Crys-

*Correspondence: robert.love@pfizer.com

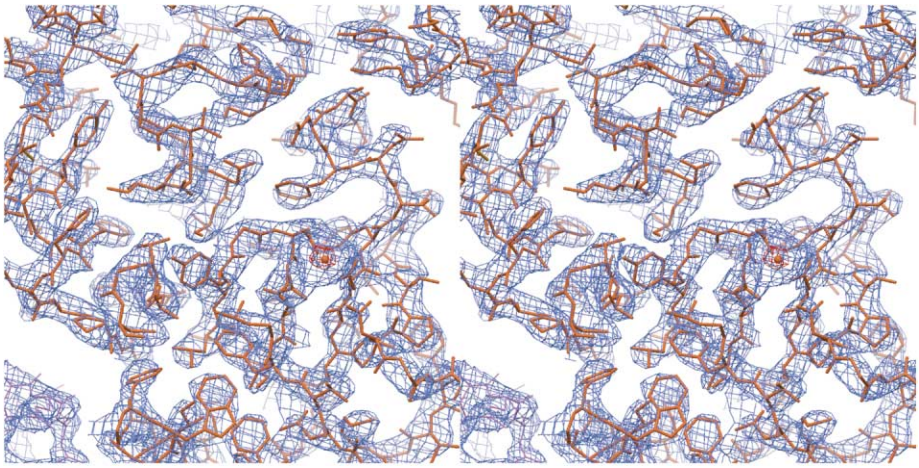

Figure 1. Experimental Density Map for HRV 3D^{pol}

Stereoview of the 2.8 Å SAD electron density map for HRV14 3D^{pol} in the vicinity of the active site (contoured at 2σ), derived from SHARP using the anomalous signal of bound samarium (red sphere). The refined structure of HRV14 3D^{pol} is superimposed.

tals of a 3D^{pol}-samarium (Sm^{3+}) complex showed an anomalous signal of sufficient strength to use single wavelength anomalous dispersion (SAD; see Experimental Procedures). The resulting electron density map provided an essentially continuous trace for all 460 amino acids, with density visible for most of the larger side chains (Figure 1). Only in regions corresponding to residues 18–22, 47–54, and 130–138 did the map display some ambiguity, likely due to flexibility and/or multiple conformations. After a model for HRV14 3D^{pol} was constructed and refined at 2.8 Å, it was used for molecular replacement to determine the structures of HRV1B and HRV16 3D^{pol} (each about 50% homologous with HRV14), which crystallize in different space groups. HRV1B and HRV16 3D^{pol} were refined at 2.5 and 2.3 Å, respectively. Data collection and refinement statistics are shown in Table 1.

Overall Structure of HRV 3D^{pol}

The crystal structure of HRV 3D^{pol}, as represented by serotype HRV1B, is shown in Figure 2. The structures for the three serotypes of the enzyme were determined from different space groups but superimpose closely (Figure 3A). The Cα atom root-mean-square deviation (rmsd) is 0.9 Å between HRV1B and HRV16 (85% sequence identity) and 1.1 Å between either HRV1B or HRV16 and HRV14 (52% sequence identity). The largest differences involve exterior residues and thus could arise from crystal packing as well as sequence variation. HRV 3D^{pol} displays the typical "right hand" arrangement of fingers, palm, and thumb domains observed in most polynucleotide polymerases (Steitz, 1999), and its folding topology resembles that of RdRps from HCV (Ago et al., 1999; Bressanelli et al., 1999; Lesburg et al., 1999) and RHDV (Ng et al., 2002) despite less than 10% and 20% sequence identity, respectively (Figure 3B). Superposition of topologically equivalent secondary structure results in a rmsd of 3.63 Å between HRV1B 3D^{pol} and HCV NS5B (220 Cα atoms), or 2.36 Å with RHDV RdRp (252 Cα atoms). HRV 3D^{pol} has significantly less structural similarity with the polymerases from BVDV (Choi et al., 2004) and bacteriophage ϕ6 (Butcher et al., 2001).

As expected, HRV 3D^{pol} most closely resembles the picornaviral poliovirus 3D^{pol} enzyme (Hansen et al., 1997), except at the N terminus (Figure 4A). Excluding PV residues 12–25, superposition of the two gives a rmsd (on 286 Cα atoms) of 1.14 Å for HRV14 (64% identity), 1.18 Å for HRV16 (56% identity), and 1.12 Å for HRV1B (57% identity). However, the crystal structure of PV 3D^{pol} shows extensive disorder in the fingers domain, whereas this domain is fully ordered in all three HRV serotypes. The complete view offered by HRV 3D^{pol} confirms a conservation of tertiary structure among RdRps from diverse RNA viruses, supporting an evolutionary relationship between picornaviruses, flaviviruses, caliciviruses, and even double-stranded RNA viruses. Significant differences in detailed secondary structure that remain between these polymerases may reflect not only substrate diversity but also divergent mechanisms for the initiation of RNA synthesis (primer dependent for HRV and RHDV but primer independent for HCV and ϕ6).

Descriptions of Individual Domains

The fingers domain of HRV 3D^{pol} (1-200, 243-290) can be divided into an N-terminal segment containing the first 54 residues (prior to α helix α2), an "inner" region surrounding the palm domain, and an "outer" region projecting away from the palm (Figure 2). The N-terminal segment displays limited secondary structure, and serves as a bridge reaching across to form numerous interactions with the adjacent thumb domain, for example through helix α1 (30-33). The first seven residues form β strand β1, which defines one edge of a five-stranded β sheet comprising the core of the outer fingers domain. Deletion of the first six residues in PV 3D^{pol} inactivates the enzyme (Hobson et al., 2001), possibly due to a loss of N-terminal anchoring and/or disruption of the fingers domain β sheet. The fold of the HRV N-terminal segment, which resembles that of RHDV and HCV, is a feature observed thus far only in the RdRp

Table 1. Crystallographic Data and Refinement Statistics

HRV Serotype	HRV-14/Sm^{3+}	HRV-1B	HRV-16
Crystal Data			
Space group	$P3_121$	$P3_221$	$P2_12_12_1$
Unit cell (a, b, c in Å)	97.3, 97.3, 153.1	88.4, 88.4, 186.2	100.98, 100.96, 116.84
Diffraction Data[a]			
X-ray source	APS 17ID	ALS 5.0.1	ALS 5.0.1
Wavelength (Å)	1.844	1.0	1.0
Resolution range (Å)	99–2.8	20–2.5	25–2.3
Observations	191,855	230,520	279,594
Unique reflections	36,073[b]	30,009	53,177
Completeness (%)	89 (32)	99 (99)	99 (99)
$< I/\sigma_I >$	15 (1.3)	17 (4.4)	15 (5.5)
R_{sym} (%)[c]	10.2 (40.6)	9.5 (54.8)	7.4 (34.2)
Anomalous difference (%)	8.5	—	—
Structure Refinement			
Resolution range (Å)	20–2.8	20–2.5	20–2.3
Reflections used	18,615	28,456	50,371
R factor, R_{free} (%)[d]	25.9, 27.7	23.1, 26.6	25.2, 28.5
Protein atoms	3679	3688	7384
Solvent/metal atoms	2/1	253/1	205/0
Average B ($Å^2$)	56.8	31.1	28.2
Rmsd bond lengths (Å)	0.012	0.010	0.011
Rmsd bond angles (°)	1.40	1.21	1.29

[a] Values in parentheses refer to the highest resolution shell.
[b] Friedel pairs were counted as independent for HRV14 only.
[c] $R_{sym} = \Sigma|< I > - I|/\Sigma I$, where I is measured intensity for reflections with indices hkl.
[d] R factor $= 100 \times \Sigma|F_o - F_c\ I|/\Sigma|F_o|$; R_{free} = free R factor based on random 5% of all data

family. In PV $3D^{pol}$ only part (12–37) of the N terminus is observed, and while residues 24–37 align closely with HRV, residues 12–23 are oriented into the enzyme's active site cavity (Figure 4A). Interestingly, the region of greatest ambiguity (and likely flexibility) in HRV $3D^{pol}$ occurs at residues 18–22 (an analogous region exists in RHDV RdRp), thus similar flexibility in PV may account for its unusual N-terminal configuration. Residues 38–66 of PV $3D^{pol}$ are disordered (along with fingers domain 98–181), and it was proposed that residues 12–37 might originate from a neighboring molecule via N-terminal exchange (Hansen et al., 1997). This was based on the concern that residues 38–66 would otherwise extend 45 Å across the top of the active site cleft. However, based on HRV $3D^{pol}$ and related HCV and RHDV enzymes, such bridging appears to be a common characteristic of RdRps. An intramolecular interpretation of the PV $3D^{pol}$ crystal structure was presented recently (Cameron et al., 2002). Nevertheless, biochemical cross-linking experiments have provided some support for an interstrand exchange model of PV polymerase interaction (Hobson et al., 2001).

The "inner fingers" region of HRV $3D^{pol}$ consists primarily of helices α3, α9, α10, α13, and α14 which surround and pack against the palm domain. All of these helices are visible in the PV $3D^{pol}$ structure, and have structural homology with helices in HCV and RHDV RdRps. The "outer fingers" region of HRV $3D^{pol}$ includes (i) a five-stranded β sheet (β1, β6, β8, β10, β11) capped by surface-exposed helices α5, α6, and α7, (ii) an adjacent helix α4 and β-hairpin β4-β5, and (iii) a loop formed by β7 and α8 (160-173) which effectively extends strands β6 and β8 toward the thumb domain to provide support for the bridging N-terminal motif; all of the homologous residues in the PV $3D^{pol}$ crystal structure are disordered. The central β sheet forming the core of the outer fingers is a common theme among RdRps, although the number of strands varies from four (BVDV) to five (HCV, ϕ6, HRV) to six (RHDV). Strand β8 contains motif F (residues 172–176), which is unique to the RdRp class (Ago et al., 1999; Bressanelli et al., 1999; Lesburg et al., 1999) and is defined as Arg-X_n-Ile/Leu (n = 1, 2). Highly conserved Arg174 of HRV (Arg188 in RHDV, Arg158 in HCV) corresponds to Arg72 of HIV-RT, which interacts with the α-phosphate of the nascent NTP (Huang et al., 1998).

A topological feature of HRV $3D^{pol}$ potentially unique to picornaviral RdRps is the β-hairpin defined by β4-β5 (residues 102–104 and 107–109), immediately following α4 (a helix common to HRV, RHDV, and HCV RdRps). This hairpin likely exists in PV $3D^{pol}$ based on sequence comparisons, although it falls within the disordered region of that crystal structure. It also represents the only significant sequence insertion in HRV $3D^{pol}$ relative to RHDV RdRp (Figure 6). Hairpin β4-β5 has an interesting similarity with β-loop β17-β18 (443-454) of HCV NS5B, although the latter emerges from the "opposite" (thumb) side of the protein and partially blocks the active site cavity. It has been proposed that the NS5B β-loop repositions to serve as a "guide" for duplex RNA (Lesburg et al., 1999).

The palm domain of HRV $3D^{pol}$ (201-242, 291-373) shows the greatest structural similarity to other polymerases, particularly PV $3D^{pol}$, and is defined by central β sheet β9, β12, β13 surrounded by helices α11, α15, and

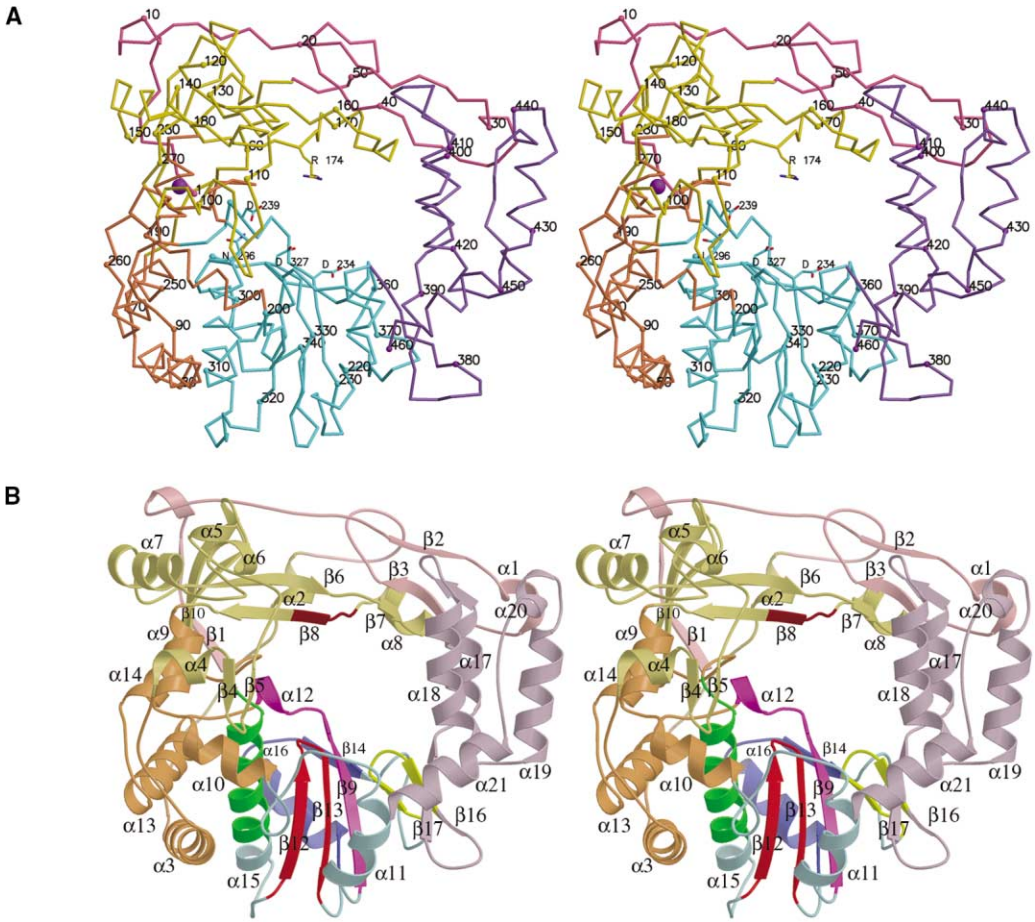

Figure 2. Structural Features of HRV 3D^{pol}

(A) Stereo Cα trace of HRV1B 3D^{pol} showing side chains of amino acids which are highly conserved among RNA-dependent RNA polymerases. The fingers domain (1–200, 243–290) is composed of the N-terminal 54 residues (violet), the "outer fingers" (gold), and the "inner fingers" (orange). The other major domains are the palm (cyan; 201–242, 291–373) and the thumb (purple; 374–460). The proposed potassium binding site is indicated by the purple sphere.

(B) Stereo ribbon representation of secondary structure for HRV1B 3D^{pol} with coloring scheme for domains as described above, but additionally highlighting conserved polymerase motifs as follows: motif A (magenta; 229–241), motif B (green; 291–308), motif C (red; 319–334), motif D (blue; 338–355), motif E (yellow; 368–378), and motif F (brown; 172–176).

α16. This domain includes most of the conserved motifs identified for oligonucleotide polymerases (Figure 2B). Motif A (229-241) is defined by β9 and α12 and features conserved Asp234, one of the primary magnesium coordination residues required for catalysis. Motif A also contains Asp239, which likely plays a key role in discriminating between ribonucleotides and 2′-deoxyribonucleotides in RdRps by hydrogen bonding to the 2′-OH of NTP (Hansen et al., 1997). Motif B (291-308) includes most of helix α15, along with highly conserved Asn296, which hydrogen bonds to Asp239 and presumably positions the latter for NTP recognition (Hansen et al., 1997). Motif C (319-334) is a highly conserved feature among polymerases, involving β-turn-β motif β12-β13 and the GDD sequence (326-328) found in the majority RdRps. Asp327 and Asp234 are absolutely required for the nucleotidyl transfer reaction and are responsible (along with the phosphates of NTP) for chelation of two magnesium ions at the active site. Motif D (338-355) is formed by α16 and β14 and provides structural support for motif A. Motif E (368-378) is defined by β-hairpin β15-β16 joining the palm and thumb domains, and along with motif F is unique to the RdRp family.

The thumb domain of HRV 3D^{pol} (residues 374–460) is formed by four long helices α17, α18, α19, and α21 and short helix α20, all of which superimpose well onto PV 3D^{pol} (Figure 4A). The folding topology of the HRV 3D^{pol} thumb is generally similar to RHDV enzyme except that the latter lacks short helix α20 and contains a long insert between its first and second helices. While the HRV and PV 3D^{pol} thumb domains present a compact helix-bundle appearance, the HCV NS5B thumb is significantly larger due to three additional helices following HRV α21, and to a β-hairpin inserted between the third and fourth helices as described above. Finally, while the crystal structures of HRV and RHDV 3D^{pol} represent the complete functional protein, HCV has an additional C-terminal transmembrane segment not included in constructs used for crystallization studies (Ago et al., 1999; Bressanelli et al., 1999; Lesburg et al., 1999).

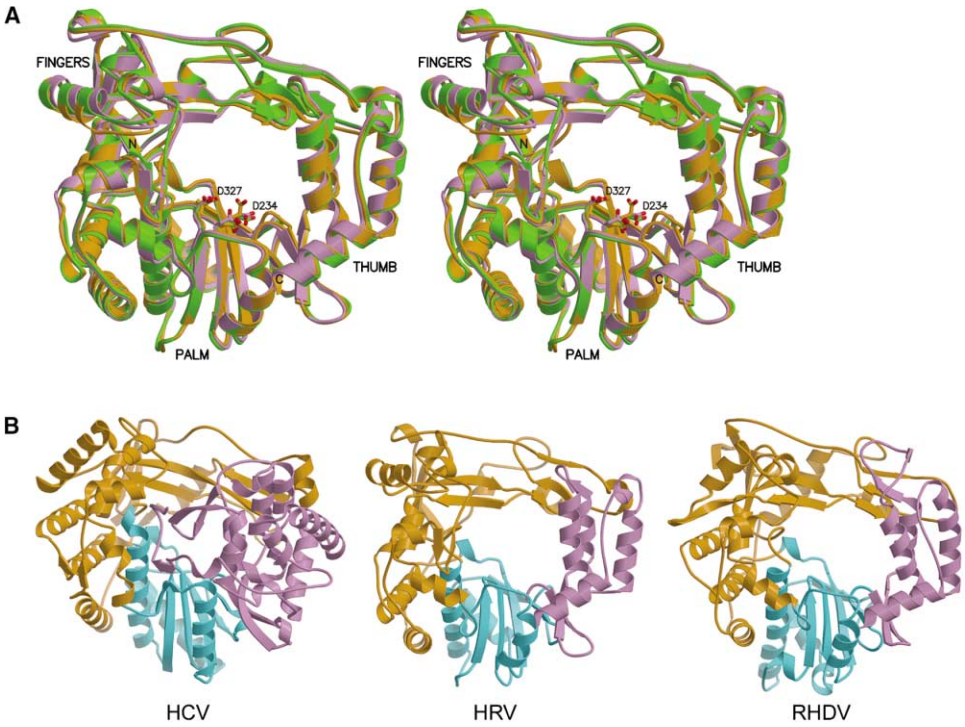

Figure 3. Similarity of 3D^{pol} among HRV Serotypes and to Other RNA-Dependent RNA Polymerases

(A) Stereo superposition of 3D^{pol} from serotypes HRV1B (purple), HRV16 (green), and HRV14 (orange). The three structures are very similar overall, with no domain rotations and only small local variations located primarily in the fingers domain.

(B) Hepatitis C virus NS5B (left), human rhinovirus 3D^{pol} (middle), and rabbit hemorrhagic disease virus polymerase (right) display a similar overall fold despite very low sequence homology. Finger, palm, and thumb domains of each enzyme are colored orange, cyan, and purple, respectively. The generally spherical shape of each molecule results from the bridging of finger and thumb domains, which is unique to the RNA-dependent RNA polymerase (RdRp) class.

Potassium Binding Site

During crystallographic refinement of HRV1B 3D^{pol}, a potential monovalent cation binding site was identified at the boundary between the inner and outer fingers domains (Figures 2A and 5B), based on the type and arrangement of coordinating ligands (four main chain carbonyl oxygens and one serine side chain), cation-oxygen distances, and atomic temperature factors (see Experimental Procedures). The local geometry of this site is preserved in HRV14 and HRV16 3D^{pol} yet only a water molecule is present. HRV1B crystallization employed high concentrations of potassium and sodium, while HRV14 and HRV16 crystallization involved concentrated sodium and/or ammonium salts; therefore, K^+ was selected as the cation most likely bound to HRV1B. Consistent with this choice is the finding that the enzyme's polymerase activity is significantly higher in assay buffer containing potassium ions relative to one with sodium ions (see Experimental Procedures). Furthermore, at low concentrations potassium has a modest stimulatory effect on HRV 3D^{pol} polymerase activity (Hung et al., 2002). It is unknown whether or not potassium is bound to the enzyme in a cellular environment.

The proposed potassium site in HRV 3D^{pol} is about 15 Å from the catalytic residues and does not appear to be directly involved in polymerase activity or RNA binding. The cation more likely plays a structural role by stabilizing one end of the fingers domain β sheet (which includes the N terminus). The site is also adjacent to conserved motifs A and B and thus may influence their positions relative to RNA substrate. Prediction of potassium binding in PV 3D^{pol} is complicated by the fact that the potential site lies within the disordered region of the structure, and that PV has an insertion of one residue at position 268 relative to HRV sequences (Figure 6). Specifically bound monovalent cations have been located in numerous crystal structures, where both functional and structural roles have been assigned. In particular, stabilizing roles for potassium ions have been deduced from the structures of AICAR transformylase (Greasley et al., 2001), tryptophanase (Isupov et al., 1998), dialkylglycine decarboxylase (Toney et al., 1993), and rabbit muscle pyruvate kinase (Larsen et al., 1994).

Metal Binding at the Active Site

Conserved aspartic acids in polymerase palm domains ligate the two magnesium ions needed for the polymerization reaction, with one metal activating the primer 3′-OH for attack of the nucleotide α-phosphate, and the other metal serving to stabilize the triphosphate moiety. Although it was not possible to obtain HRV 3D^{pol} crystals with bound divalent cations and NTP, in HRV14 3D^{pol}-samarium cocrystals the metal (Sm^{3+}) was found to occupy the position expected for the Mg^{2+} denoted "A" (closest to the primer 3′-OH), with coordination by Asp327 and Asp328 from motif C and Asp234 from motif

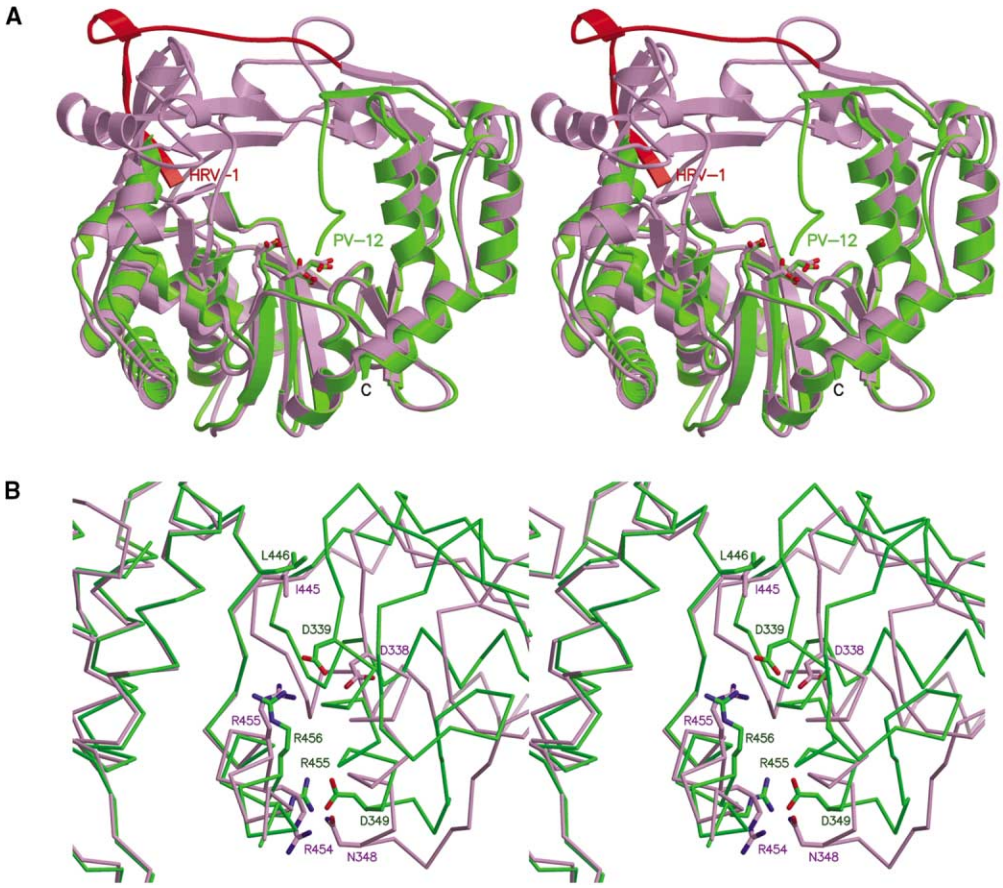

Figure 4. Comparison of HRV and PV 3D^{pol}

(A) Stereoview of poliovirus (PV) 3D^{pol} (green) superimposed on HRV1B 3D^{pol} (purple, red), with Cα atom rmsd of 1.1 Å (excluding 12–25 of PV). The N-terminal 25 residue segment (colored red in HRV) adopts very different positions in the two crystal structures, but the configuration in HRV 3D^{pol} is similar to the folding topology of HCV, RHDV, and ϕ6 polymerases.

(B) Stereoview of intermolecular contacts in poliovirus 3D^{pol} crystals designated "interface I" (green), which have been proposed to explain oligomerization of the enzyme observed biochemically. PV thumb residue Leu446 inserts into a hydrophobic pocket on the palm of a neighboring molecule, while two salt bridges (Arg456-Asp339 and Arg455-Asp349) stabilize a helix-helix contact. In HRV14 3D^{pol} crystals (but not HRV16 or HRV1B), a similar interface (purple) entails Ile445 fitting into an adjacent pocket, but analogous salt bridges do not form due to a molecular rotation that separates HRV14 Arg455 and Asp338, and also to the substitution of HRV14 Asn348 for PV Asp349. There is currently no evidence that protein oligomerization plays a role in the function of HRV 3D^{pol}.

A (Figure 5A). The resulting side chain configuration around Sm^{3+} is very similar to HCV NS5B plus bound Mg^{2+} or Mn^{2+} (Ago et al., 1999; Bressanelli et al., 1999; O'Farrell et al., 2003) and with the exception of Asp328, to RHDV RdRp plus bound Lu^{3+} or Mn^{2+} (Ng et al., 2002) or HIV-RT plus bound Mg^{2+} (Huang et al., 1998). In HRV14 3D^{pol} there appears to be additional electrostatic interaction between conserved Asp357 and bound Sm^{3+} (distance ~4.9 Å). Comparison of HRV14 3D^{pol} structures obtained with and without Sm^{3+}, and comparison of HRV14/Sm^{3+} to unbound HRV16 or HRV1B enzymes, shows that the binding of the metal causes shifts of strand β9 (containing Asp234) and parallel strand β14 (containing Asp357) inward toward the metal (Figure 5A). These relatively small differences between Sm^{3+}-bound and apo HRV 3D^{pol} mirror those found between Mn^{2+}/Lu^{3+}-bound and apo RHDV RdRp, and the two states of RHDV have been termed a "closed" and "open" conformation, respectively (Ng et al., 2002).

No global conformational change was observed upon binding of a metal at the active site of HRV 3D^{pol}, consistent with findings from several HCV NS5B structures containing bound metals and NTP (Ago et al., 1999; Bressanelli et al., 1999; O'Farrell et al., 2003). Since HRV14 3D^{pol} was crystallized in the presence or absence of samarium independently, large-scale changes associated with lanthanide binding were potentially detectable, yet the HRV14/Sm^{3+} complex aligns very closely with apo HRV14, HRV1B, and HRV16. For RHDV RdRp, one molecule in the asymmetric unit displays a rotation of the thumb domain inward about 8° toward the palm domain (likely due to crystal packing forces), and only this copy contains the "closed" configuration of aspartic acids with bound metal(s). Therefore in some RdRps small domain rotations may be required to stabilize a conformation competent for binding metals and NTP, although the ATP present in RHDV crystals was not resolved in the final structure. The absence of bound ATP or Mg^{2+} in HRV16 3D^{pol} (despite cocrystallization) could imply a need for additional protein rearrangement

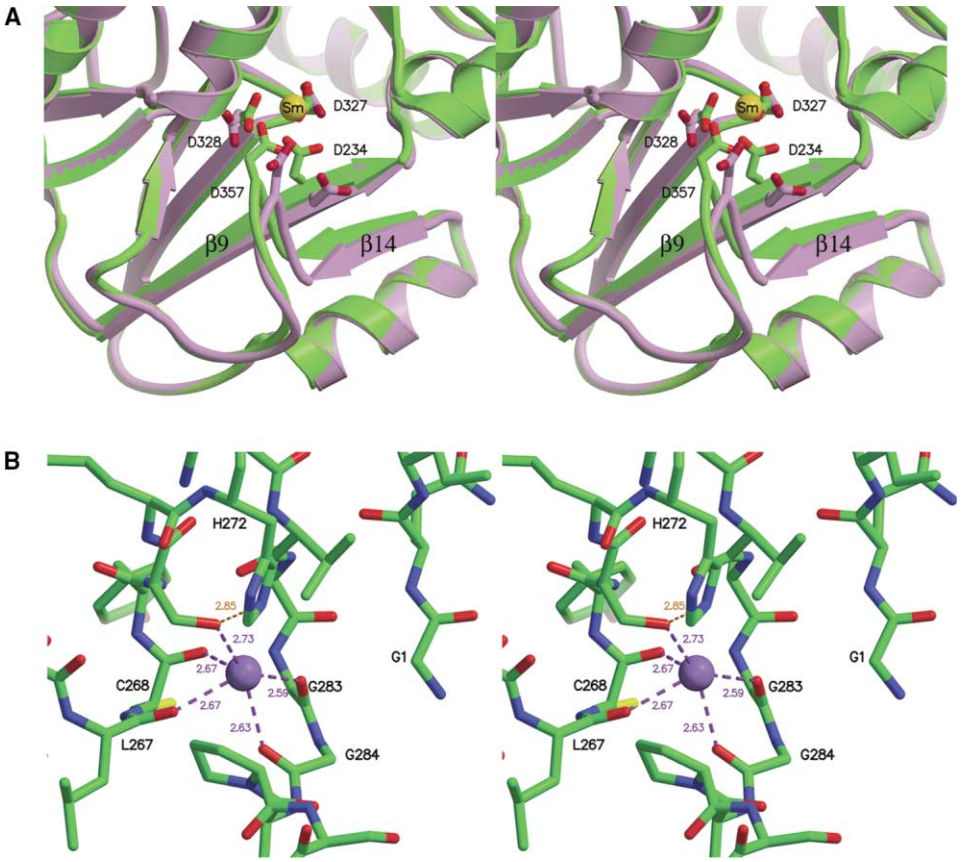

Figure 5. Ion Binding Sites in HRV 3D^{pol}

(A) Stereo comparison of the HRV14 3D^{pol} structure without (purple) and with (green) bound Sm^{3+} (yellow sphere) at the active site. The structures are essentially identical except for recruitment of Asp234 for metal chelation, shifts of strands β9 and β14 inward, and rotation of Asp357 toward the metal. Similar shifts have been observed in RHDV RdRp upon binding of Lu^{3+} or Mn^{2+} at the active site.

(B) Stereoview of a potential potassium binding site observed in the HRV1B 3D^{pol} crystal structure. This irregular penta-coordination scheme is preserved in the HRV14 and HRV16 3D^{pol} structures but only a water molecule is present, possibly due to crystallization conditions which lacked the concentrated potassium used for HRV1B.

and/or simultaneous binding of primer-template RNA. In any case, large-scale conformational changes do not appear critical for the functioning of RdRps, unlike other polymerase classes (Doublie et al., 1999), possibly due to rigidity provided by the tight interaction of thumb and finger domains. Structures of RdRps complexed with RNA duplexes will be needed in order to determine whether a more open enzyme conformation is required for substrate binding and elongation.

Potential Oligomerization Interfaces

Within the crystal lattice of PV 3D^{pol}, molecules interact through two extensive contact surfaces referred to as interface I and interface II (Hansen et al. 1997), giving rise to higher order structures that have been proposed to explain oligomerization observed biochemically (Beckman and Kirkegaard, 1998; Pata et al., 1995) and large sheets and tubes observed by electron microscopy (EM) using purified enzyme or vesicles from PV-infected cells (Lyle et al., 2002a). Interface I involves the back of the palm interacting with the back of the thumb on an adjacent molecule, defining "head-to-tail oligomeric fibers" running through the crystal. Interface II, which potentially involves intermolecular strand exchange, forms another set of fibers running about 90° relative to the first. Based on the conservation of residues defining each interface, it has been hypothesized that interface I could be a feature of most picornavirus polymerases (Cameron et al., 2002). Disruption of contacts forming interface I in PV 3D^{pol} crystals by site-directed mutagenesis diminishes biochemically detected oligomerization (Hobson et al., 2001; Pathak et al., 2002) and reduces higher order EM structures (Lyle et al., 2002a).

Of the three serotypes of HRV 3D^{pol} presented here, which crystallize in different space groups, none form crystal lattice contacts resembling interface II of PV 3D^{pol}. Futhermore, neither HRV16 nor HRV1B 3D^{pol} show interactions found in interface I of PV. However, crystals of HRV14 3D^{pol} contain an intermolecular contact similar to interface I, in that the side chain of Ile445 (corresponding to PV Leu446) packs into a hydrophobic pocket on the back of the palm of a symmetry-related molecule (Figure 4B). This HRV14 pocket is formed by residues Ile308, Tyr312, Ile315, Tyr335, and Leu337 (homologs of PV Leu309, Tyr313, Ile316, Tyr334, and Val338, respec-

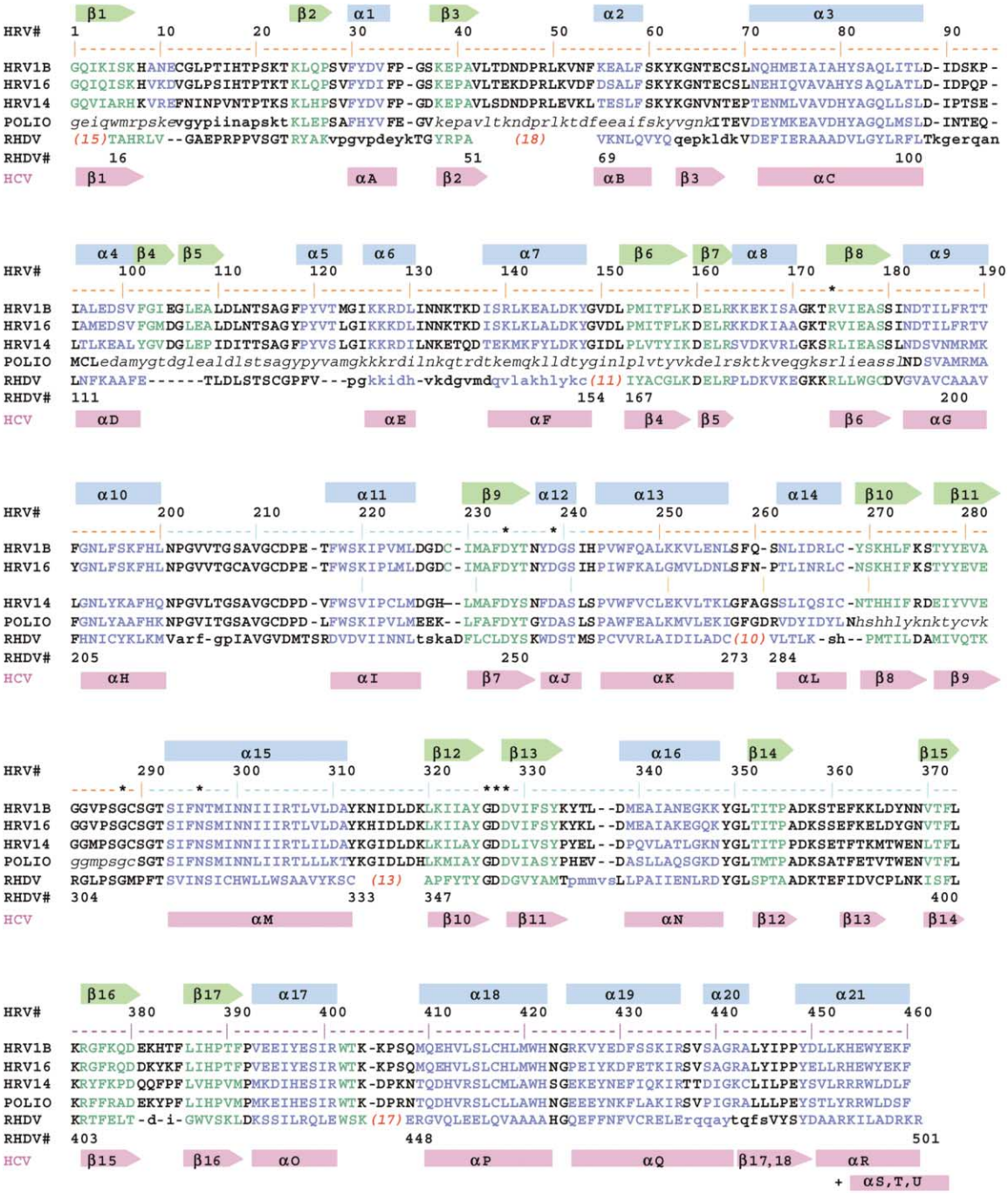

Figure 6. Structure-Based Alignment of HRV 3D^{pol} Sequences with Other RdRps

Alignment of HRV 3D^{pol} sequences for serotypes 1B, 16, and 14 with those of RdRps from poliovirus (PV) and rabbit hemorrhagic disease virus (RHDV, see separate numbering scheme). Secondary structure common to HRV/PV/RHDV is indicated on top, and correlated secondary structure from HCV NS5B polymerase is shown below using nomenclature of Bressanelli et al. (1999). Residues which are highly conserved across RdRp's are highlighted with an asterisk. Regions of RHDV or PV which show a significantly different conformation relative to HRV are indicated by bold, lower case letters. Disordered residues of PV are indicated by plain lower case letters. Residues of RHDV which represent significant insertions relative to HRV (≥5 residues) are indicated by a number in parentheses (red); these insertions occur as surface features on the periphery of the enzyme (far from active site residues). The major polymerase structural domains are denoted by colored dashes above the sequences: fingers (orange), palm (cyan), and thumb (purple). (Note: following PV Asn269, the top numbering scheme should be incremented by one to obtain the corrected PV residue number.)

tively). However, two salt bridges which complete interface I in PV, linking thumb helix α21 (Arg455, Arg456) of one molecule to palm helix α16 (Asp349, Asp339) of another, are not formed in HRV14 crystals due to a longer distance between the helices (separating HRV14 Arg455 and Asp338), and to the substitution of HRV14 Asn348

for PV Asp349. This difference is reflected in the buried surface area at interface I, which is 1480 Å^2 for PV (Hansen et al., 1997) but only 1010 Å^2 in HRV14. Nevertheless, the HRV14 interface is large enough to suggest a homodimeric state for the enzyme in solution, based on statistical analysis of crystal packing interfaces (Ponstingl et al., 2000).

It is unclear whether the crystal contacts in HRV14 3D^{pol} would be sufficient to promote protein oligomerization analogous to PV 3D^{pol}, since such a phenomenon has not been reported for any serotype of HRV 3D^{pol}. Our samples of purified HRV 3D^{pol} show modest aggregation by light scattering analysis, and small amounts of detergent are used for assays and crystallization (see Experimental Procedures), but the nature of this aggregation is not understood. In the case of PV, recent studies suggest that the capacity of 3D^{pol} to form oligomers or fibers is not essential for virus multiplication (Pathak et al., 2002).

Modeling of Oligonucleotide Substrate

A variety of bound ligands have been visualized in polymerase crystal structures, but within the RdRp class these are limited to nucleotides and/or divalent metals (Ago et al., 1999; Bressanelli et al., 1999; Butcher et al., 2001; Choi et al., 2004; Ng et al., 2002; O'Farrell et al., 2003), a short single-stranded RNA oligomer (O'Farrell et al., 2003) or DNA oligomer (Butcher et al., 2001), and a few small molecule inhibitors (Love et al., 2003; Wang et al., 2003), rather than duplex RNA. However, given the structural similarity of the palm domain among polymerases, it is possible to create a model of HRV 3D^{pol} (starting from HRV14/Sm^{3+}) containing bound primer-template, NTP, and Mg^{2+}, guided by the experimental HIV-RT/DNA/dNTP/Mg^{2+} complex (Huang et al., 1998) and also the RHDV RdRp/Mn^{2+} complex (Ng et al., 2002). As in most polymerase-DNA complexes, the DNA duplex bound to HIV-RT displays an A-like conformation in the vicinity of the polymerase active site and thus may approximate an RNA substrate (Doublie et al., 1999). HIV-RT DNA also features a slight bend which allows it to fit into HRV 3D^{pol} with few steric clashes, unlike the result from docking linear DNA or RNA derived from nucleic acid crystal structures. The resulting position of the template strand in the HRV 3D^{pol}-duplex model overlaps that of a short RNA oligomer bound to HCV NS5B (O'Farrell et al., 2003) or a short DNA oligomer bound to bacteriophage ϕ6 (Butcher et al., 2001).

In the HRV 3D^{pol} model, each of the three polymerase domains plays a significant role in supporting the primer-template duplex by interacting with the sugar-phosphate backbone (Figure 7). A particularly interesting result is that hairpin β4-β5 appears poised to fit into the major groove, possibly serving as guide for the duplex analogous to the role proposed for loop β17-β18 in the thumb of HCV NS5B (Lesburg et al., 1999). HRV residues 18–22 and 130–138, which show relatively high mobility in the crystal structures, are located near the expected "entry" of the template strand (5′ end) and "exit" of the primer strand (5′ end), where protein flexibility may be advantageous for optimizing enzyme-duplex interactions.

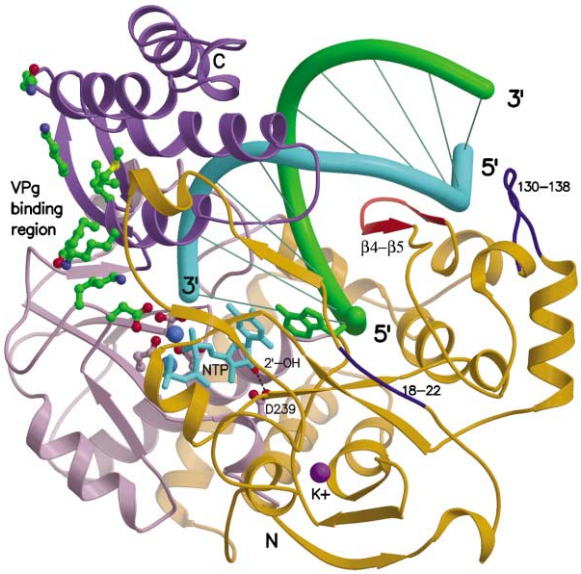

Figure 7. Duplex Oligonucleotide Modeled into HRV 3D^{pol}

This model combines the HRV14/Sm^{3+} 3D^{pol} structure with the primer-template (cyan and green ribbons), NTP (cyan), and Mg^{2+} (blue spheres) from the HIV-RT/DNA/dNTP/Mg^{2+} complex (Huang et al. 1998). The dNTP molecule from HIV-RT was converted to rNTP, but for this approximation the primer-template backbone was retained as 2′-deoxyribose. HRV 3D^{pol} domains are colored according to fingers (orange), palm (violet), and thumb (purple). Asp239 (labeled) is positioned to hydrogen bond to the 2′-OH group of NTP, providing ribonucleotide discrimination. β-hairpin β4-β5 (red) appears poised to interact with the major groove of the duplex, possibly serving as a "guide" analogous to the role proposed for β-loop β17-β18 of HCV NS5B. Relatively flexible HRV residues 18–22 and 130–138 (blue) are located near the template entry point (5′ end) and primer exit point (5′ end). The structural potassium binding site inferred from the HRV1B structure is indicated by the purple sphere. Also shown are residues (green side chains) which, based on studies of homologous PV 3D^{pol}, contribute to binding and uridylylation of the primer peptide VPg.

The HRV model predicts several contacts between NTP and basic amino acids which are highly conserved among RdRps. Positioned to interact with the triphosphate moiety of NTP is Arg174 (Arg174 in PV 3D^{pol}, Arg188 in RHDV RdRp, Arg72 in HIV-RT, and Arg158 in HCV NS5B). Lys167 probably assists Arg163 in playing a role similar to the single basic residue Lys65 of HIV-RT, Lys155 of HCV NS5B, or Arg177 of RHDV RdRp. Arg163, Lys167, and Arg174 are disordered in PV 3D^{pol} but presumably would have positions similar to those in HRV. The model also implies hydrogen bonding between NTP 2′-OH and highly conserved Asp 239, which is likely responsible for ribonucleotide recognition within the RdRp family (Hansen et al., 1997). Similar interactions between PV 3D^{pol} and NTP have been modeled (Gohara et al., 2000).

Other Picornaviral Polymerase Functions

The 5′ end of picornaviral RNA is found linked to a small virally encoded peptide 3B (or VPg), which is believed to function as a protein primer for RNA replication. In vitro, 3D^{pol} from PV or HRV can catalyze the formation of a phosphodiester bond between UMP and the hy-

droxyl of VPg Tyr3, in the presence of UTP and an RNA template (Gerber et al., 2001; Paul et al., 1998). The RNA template for this VPg uridylylation is a small stem-loop structure termed a "*cis*-replicating element" (*cre*), which is located within the viral coding sequence and contains a conserved AAACA motif (Goodfellow et al., 2000; McKnight and Lemon, 1998). Mutational analysis of PV 3D^{pol} (Lyle et al., 2002b) has identified several surface residues whose substitution reduces both VPg binding affinity and rate of VPg uridylylation (PV Arg379, Glu382, Val391, and Phe377, corresponding to HRV14 Lys378, Gln381, Val390, and Phe376), or reduces the VPg uridylylation rate alone (PV Asp358, Lys359, Met394, and Lys395, corresponding to HRV14 Asp357, Lys358, Met393, Lys394). These residues define a patch on the 3D^{pol} surface over which the VPg peptide would likely interact, allowing the VPg tyrosine side chain to enter the active site where UTP resides (Figure 7). During the uridylylation reaction, the RNA stem-loop *cre* template would probably occupy the same general position as the primer-template in the replication complex.

Conclusions

Inhibition of virally encoded enzymes has become an important strategy to develop new antiviral agents, particularly in cases where vaccine development has been unsuccessful. The RdRp of rhinovirus represents a particularly interesting target because of its dual functions of viral RNA synthesis and protein primer synthesis. The crystal structure of HRV 3D^{pol} provides the first complete picture of a polymerase from the picornavirus family. Its overall architecture fits the expected theme of polymerase fingers/palm/thumb domains, and supports an evolutionary conservation of tertiary structure among RdRps from diverse RNA viruses. HRV 3D^{pol} also reveals several unexpected features, such as a structural potassium binding site and a β-hairpin that appears unique to picornaviral RdRps and may guide the nascent RNA. The previously proposed ridigity of RdRp enzymes, inferred from their intimate fingers-thumb interaction and modest change upon ligand binding, is supported here by the similarity of HRV 3D^{pol} structures from three serotypes in different crystal forms, and by a comparison of the structure with and without bound metal. While a cocrystal structure with RNA will be necessary in order to fully resolve questions of flexibility, an RNA-like primer-template duplex can be modeled into the HRV 3D^{pol} crystal structure without severe steric consequences.

Experimental Procedures

Protein Expression and Purification

HRV 3D^{pol} genes encoding serotypes HRV14, HRV16, and HRV1B were cloned into *E. coli* expression plasmids, which were then transformed into *E. coli* strain BL21(DE3). Expression was induced by IPTG for 4 hr at 25°C. Each serotype is comprised of 460 amino acids (~52 kDa). HRV14 protein had a C-terminal six-histidine tag, and was purified by Ni-NTA, Sephadex G75, and poly(U) Sepharose chromatography columns, then stored in a buffer containing 20% glycerol, 20 mM HEPES, pH 8.0, 150 mM NaCl, and 10 mM DTT. HRV1B and HRV16 proteins were purified by SP Sepharose and poly(U) Sepharose chromatography columns, and stored in a buffer containing 10% glycerol, 25 mM HEPES, pH 8.0, 150 mM NaCl, and 5 mM DTT. Mass spectrometry analysis of purified proteins yielded the expected molecular weights, and N-terminal sequencing confirmed the first amino acid as glycine rather than methionine.

Biochemical Assays

RNA-dependent RNA polymerase activity of purified HRV 3D^{pol} was verified by combining 50 μM UTP, 0.33 μCi ^{33}P UTP, and rA:dT template-primer in assay buffer containing 50 mM KPO_4, pH 6.6, 10 mM KCl, 1 mM $MgCl_2$, 2.5 mM DTT, 0.05% Tween-20 in a 50 μl reaction. The template-primer was made by annealing biotinylated 17-mer dT primers to poly rA (Amersham) in a 3:1 ratio of primer to template. The final concentration of primer in the assay was 100 nM. The enzymatic reaction was started with the addition of 5 nM HRV 3D^{pol}. Following incubation at 25°C for 20 min, the reaction was stopped with the addition of EDTA, 25 mM final concentration. The reaction mix was then filtered thru a Schleicher and Schuell 96-well filter unit with a DEAE glass fiber filtermat (Wallac), washed three times with 5% dibasic sodium phosphate buffer, rinsed with water, and dried. Incorporation of ^{33}P labeled UTP into the dT primer was quantitated using a PhosphorImager (Molecular Dynamics).

The use of potassium buffer and salt (KPO_4, KCl) gave higher enzyme activity relative to the sodium counterparts ($NaPO_4$, NaCl), primarily due to an increase in k_{cat}. For example, specific activity (picomoles product per minute per picomoles enzyme) for HRV1B 3D^{pol} was 2.5 ± 0.03 in sodium buffer (K_m = 25 ± 10 nM dT primer), while 12.8 ± 0.05 in potassium buffer (K_m = 72 ± 8 nM). Specific activity for HRV16 3D^{pol} was 2.2 ± 0.06 in sodium buffer (K_m = 12 ± 2 nM dT primer), while 16.6 ± 0.5 in potassium buffer (K_m = 32 ± 3 nM).

Crystallization

In order to reduce the glycerol content prior to crystallization, while avoiding aggregation of the protein as monitored by dynamic light scattering (DLS), protein samples were dialyzed into a buffer containing 50 mM potassium phosphate (pH 6.5), 150 mM NaCl, 1% nondetergent sulphobetaine NDSB-256 (dimethylbenzylammonium propane sulfonate; Calbiochem), 0.05% Tween-20, and 10 mM DTT. All crystals were grown by the hanging drop vapor diffusion method at 13°C. Equal volumes of protein and well solution were equilibrated against 1 ml well volume. Protein concentrations were typically 5–8 mg/ml for all serotypes. The HRV14 3D^{pol} crystals used for structure determination were obtained using 3.0–3.5 M sodium formate (pH 7.0), 5%–8% glycerol, 5 mM DTT. Subsequently, other conditions provided similar crystals: (i) 1.2 M sodium citrate, 0.2 M NaCl, 0.1 M Tris-HCl pH 7.0, 10 mM DTT, and (ii) 1.0 M ammonium phosphate, 0.2 M NaCl, 0.1 M imidazole, pH 8.0, 10 mM DTT. HRV14 3D^{pol} crystals belong to space group $P3_121$ with one molecule per asymmetric unit. Soaks of the HRV14 crystals in $SmCl_3$ (or other derivatives) were not successful; only cocrystallization of the enzyme with 0.25 mM $SmCl_3$ gave crystals with a detectable anomalous signal. HRV16 3D^{pol} was crystallized in the presence of the ATP analog AMPPNP and $MgCl_2$ (or $MnCl_2$), which promoted monodispersity by DLS, although these additives were not observed in the refined structure. HRV16 conditions were 1.9 M ammonium sulfate, 0.1 M citrate, pH 5.6, 2 mM AMPPNP, 2 mM $MnCl_2$ or $MgCl_2$. Use of $MnCl_2$ tended to give a twinned $P2_1$ crystal form while $MgCl_2$ gave a closely-related but untwinned $P2_12_12_1$ form with doubled unit cell volume. These two HRV16 3D^{pol} crystal forms, which were visually indistinguishable, featured two molecules per asymmetric unit related by a pure translation, leading to a pseudotetragonal arrangement. HRV1B 3D^{pol} crystals were obtained using 1.0 M sodium potassium tartrate, 0.1 M ADA, pH 6.5, 5 mM DTT, and belong to space group $P3_221$ with one molecule per asymmetric unit.

Data Collection

Crystals were flash-frozen in Hampton loops using cryoprotectants that contained well buffer but with an additional 20%–22% glycerol. Diffraction data were collected at 100 K at either the Advanced Photon Source beamline 17ID using a Mar CCD165 detector (HRV14), or the Advanced Light Source beamline 5.0.1 using an ADSC CCD detector (HRV16, HRV1B). All data were processed with Denzo/Scalepack (Otwinowski and Minor, 1997). Data collection statistics are summarized in Table 1. An energy scan of HRV14 3D^{pol} crystals at APS led to the choice of 1.844 Å for peak absorption.

Data from an early apo-HRV14 crystal (without bound samarium) were obtained in-house at lower resolution (~3.2 Å), but these crystals could not be reproduced for synchrotron analysis.

Structure Determination and Refinement

Heavy atom parameter refinement and SAD phase calculations were performed with SHARP (De La Fortelle and Bricogne, 1997), using the anomalous signal from a single samarium atom which bound in the HRV14 $3D^{pol}$ active site at a catalytic magnesium position (f″ of 29.8 at peak absorption) The electron density map (Figure 1) was improved with solvent flattening using SOLOMON (Abrahams, 1996) as implemented in SHARP. SAD phasing statistics to 2.8 Å included a phasing power of 2.0 (0.6 in the highest shell) and an overall figure of merit before and after density modification of 0.41 and 0.78. A model was constructed for HRV14 $3D^{pol}$ using XFIT (McRee, 1992), and was refined initially with CNX (Accelrys, Inc). This model permitted the HRV1B and HRV16 $3D^{pol}$ structures to be determined with molecular replacement (CCP4, 1994). Replacement of amino acid side chains to transform HRV14 into other serotypes was performed with MODELLER (Sali and Blundell, 1993). After several rounds of XFIT and CNX for all models, REFMAC5 (CCP4, 1994) was used in final stages of refinement (maximum likelihood target). Refinement statistics are shown in Table 1. The HRV14/Sm^{3+} $3D^{pol}$ model with samarium removed was also refined against in-house 3.2 Å diffraction data obtained from a small crystal of apo-HRV14 in order to study conformational changes induced by the metal; these refinement statistics were R/R_{free} (20–3.2 Å) = 25.6/27.2, rmsd bond lengths and angles of 0.012 Å and 1.41°. Stereochemical quality of all models was checked using PROCHECK (Laskowski et al., 1993). Only Lys275 (second residue of type-II′ β-turn 274–277) was consistently an outlier in the Ramachandran plot, probably a result of salt bridges to Asp55 and Glu45 along with several main chain-main chain hydrogen bonds.

During solvent incorporation for the HRV1B $3D^{pol}$ structure, a water molecule placed into the single strongest positive peak (10 σ) of ($F_o - F_c$) maps refined to a B factor (~5 $Å^2$) much lower than the average for surrounding atoms (28 $Å^2$). Since this site involved interactions with four main chain carbonyl oxygens (average distance 2.64 Å) and a serine hydryoxyl (2.73 Å) without any regular coordination geometry, monovalent cation binding was suspected. HRV1B crystallized using 1.0 M Na-K tartrate; thus, the most likely candidates were sodium and potassium, which show an average oxygen-metal distance in small organic molecule structures of 2.4 and 2.8 Å, respectively (Cambridge Structural Database). However, only HRV1B crystallization conditions contained high levels of potassium, and the peak was not seen in HRV14 or HRV16 crystals derived from concentrated sodium and/or ammonium salts. Furthermore, our biochemical analysis of $3D^{pol}$ (see above) identified potassium as an important counterion for optimum enzyme activity. Therefore K^+ was introduced into the HRV1B $3D^{pol}$ structure and subsequently refined (using REFMAC5) to a B factor of 23 $Å^2$. Figures were generated using Molscript (Kraulis, 1991) and Raster3D (Merrit and Bacon, 1997).

Received: March 26, 2004
Revised: May 25, 2004
Accepted: May 27, 2004
Published: August 10, 2004

References

Abrahams, J.P., and Leslie, A.G.W. (1996). Methods used in the structure determination of bovine mitochondrial F1 ATPase. Acta Crystallogr. D Biol. Crystallogr *52*, 30–42.

Ago, H., Adachi, T., Yoshida, A., Yamamoto, M., Habuka, N., Yatsunami, K., and Miyano, M. (1999). Crystal structure of the RNA-dependent RNA polymerase of hepatitis C virus. Structure *7*, 1417–1426.

Beckman, M.T., and Kirkegaard, K. (1998). Site size of cooperative single-stranded RNA binding by poliovirus RNA-dependent RNA polymerase. J. Biol. Chem. *273*, 6724–6730.

Bressanelli, S., Tomei, L., Roussel, A., Incitti, I., Vitale, R.L., Mathieu, M., De Francesco, R., and Rey, F.A. (1999). Crystal structure of the RNA-dependent RNA polymerase of hepatitis C virus. Proc. Natl. Acad. Sci. USA *96*, 13034–13039.

Butcher, S.J., Grimes, J.M., Makeyev, E.V., Bamford, D.H., and Stuart, D.I. (2001). A mechanism for initiating RNA-dependent RNA polymerization. Nature *410*, 235–240.

Cameron, C.E., Gohara, D.W., and Arnold, J.J. (2002). Poliovirus RNA-dependent RNA polymerase (3Dpol): structure, function, and mechanism. In Molecular Biology of Picornaviruses, B.L. Semler and E. Wimmer, eds. (Washington, DC: ASM Press), pp. 255–267.

CCP4 (Collaborative Computational Project, Number 4) (1994). The CCP4 suite: programs for protein crystallography. Acta Crystallogr. D Biol. Crystallogr. *50*, 760–763.

Choi, K.H., Groarke, J.M., Young, D.C., Kuhn, R.J., Smith, J.L., Pevear, D.C., and Rossmann, M.G. (2004). The structure of the RNA-dependent RNA polymerase from bovine viral diarrhea virus establishes the role of GTP in de novo initiation. Proc. Natl. Acad. Sci. USA *101*, 4425–4430.

Couch, R.B. (2001). Rhinoviruses. In Fields Virology, D.M. Knipe and P.M. Howley, eds. (Philadelphia: Lippincott Williams & Wilkins), pp. 777–797.

De La Fortelle, E., and Bricogne, G. (1997). Macromolecular crystallography. Methods Enzymol. *276*, 472–494.

Doublie, S., Sawaya, M.R., and Ellenberger, T. (1999). An open and closed case for all polymerases. Struct. Fold. Des. *7*, R31–R35.

Gerber, K., Wimmer, E., and Paul, A.V. (2001). Biochemical and genetic studies of the initiation of human rhinovirus 2 RNA replication: purification and enzymatic analysis of the RNA-dependent RNA polymerase 3D(pol). J. Virol. *75*, 10969–10978.

Gohara, D.W., Crotty, S., Arnold, J.J., Yoder, J.D., Andino, R., and Cameron, C.E. (2000). Poliovirus RNA-dependent RNA polymerase (3Dpol): structural, biochemical, and biological analysis of conserved structural motifs A and B. J. Biol. Chem. *275*, 25523–25532.

Goodfellow, I., Chaudhry, Y., Richardson, A., Meredith, J., Almond, J.W., Barclay, W., and Evans, D.J. (2000). Identification of a cis-acting replication element within the poliovirus coding region. J. Virol. *74*, 4590–4600.

Greasley, S.E., Horton, P., Ramcharan, J., Beardsley, G.P., Benkovic, S.J., and Wilson, I.A. (2001). Crystal structure of a bifunctional transformylase and cyclohydrolase enzyme in purine biosynthesis. Nat. Struct. Biol. *8*, 402–406.

Greve, J.M., Davis, G., Meyer, A.M., Forte, C.P., Yost, S.C., Marlor, C.W., Kamarck, M.E., and McClelland, A. (1989). The major human rhinovirus receptor is ICAM-1. Cell *56*, 839–847.

Gwaltney, J.M., Jr., Winther, B., Patrie, J.T., and Hendley, J.O. (2002). Combined antiviral-antimediator treatment for the common cold. J. Infect. Dis. *186*, 147–154.

Hansen, J.L., Long, A.M., and Schultz, S.C. (1997). Structure of the RNA-dependent RNA polymerase of poliovirus. Structure *5*, 1109–1122.

Hobson, S.D., Rosenblum, E.S., Richards, O.C., Richmond, K., Kirkegaard, K., and Schultz, S.C. (2001). Oligomeric structures of poliovirus polymerase are important for function. EMBO J. *20*, 1153–1163.

Hofer, F., Gruenberger, M., Kowalski, H., Machat, H., Huettinger, M., Kuechler, E., and Blass, D. (1994). Members of the low-density lipoprotein receptor family mediate cell entry of a minor-group common cold virus. Proc. Natl. Acad. Sci. USA *91*, 1839–1842.

Huang, H., Chopra, R., Verdine, D.L., and Harrison, S.C. (1998). Structure of a covalently trapped catalytic complex of HIV-1 reverse transcriptase: implications for drug design. Science *282*, 1669–1675.

Hung, M., Gibbs, C.S., and Tsiang, M. (2002). Biochemical characterization of rhinovirus RNA-dependent RNA polymerase. Antiviral Res. *56*, 99–114.

Isupov, M.N., Antson, A.A., Dodson, E.J., Dodson, G.G., Dementieva, I.S., Zakomirdina, L.N., Wilson, K.S., Dauter, Z., Lebedev, A.A., and Harutyunyan, E.H. (1998). Crystal structure of tryptophanase. J. Mol. Biol. *276*, 603–623.

Johnson, T.O., Hua, Y., Luu, H.T., Brown, E.L., Chan, F., Chu, S.S., Dragovich, P.S., Eastman, B.W., Ferre, R.A., Fuhrman, S.A., et al.

(2002). Structure-based design of a parallel synthetic array directed toward the discovery of irreversible inhibitors of human rhinovirus 3C protease. J. Med. Chem. *45*, 2016–2023.

Kitamura, N., Semler, B.L., Rothberg, P.G., Larsen, G.R., Adler, C.J., Dorner, A.J., Emini, E.A., Hanecak, R., Lee, J.J., van der Werf, S., et al. (1981). Primary structure, gene organization and polypeptide expression of poliovirus RNA. Nature *291*, 547–553.

Kraulis, P.J. (1991). MOLSCRIPT: a program to produce both detailed and shematic plots of protein structures. J. Appl. Crystallogr. *24*, 946–950.

Larsen, T.M., Laughlin, L.T., Holden, H.M., Rayment, I., and Reed, G.H. (1994). Structure of rabbit muscle pyruvate kinase complexed with Mn2+, K+, and pyruvate. Biochemistry *33*, 6301–6309.

Laskowski, R.J., MacArthur, M.W., Moss, D.S., and Thornton, J.M. (1993). PROCHECK: a program to check the stereochemical quality of protein structures. J. Appl. Crystallogr. *26*, 283–291.

Lesburg, C.A., Cable, M.B., Ferrari, E., Hong, Z., Mannarino, A.F., and Weber, P.C. (1999). Crystal structure of the RNA-dependent RNA polymerase from hepatitis C virus reveals a fully encircled active site. Nat. Struct. Biol. *6*, 937–943.

Love, R.A., Parge, H.E., Yu, X., Hickey, M.J., Diehl, W., Gao, J., Wriggers, H., Ekker, A., Wang, L., Thomson, J.A., et al. (2003). Crystallographic identification of a noncompetitive inhibitor binding site on the hepatitis C virus NS5B RNA polymerase enzyme. J. Virol. *77*, 7575–7581.

Lyle, J.M., Bullitt, E., Bienz, K., and Kirkegaard, K. (2002a). Visualization and functional analysis of RNA-dependent RNA polymerase lattices. Science *296*, 2218–2222.

Lyle, J.M., Clewell, A., Richmond, K., Richards, O.C., Hope, D.A., Schultz, S.C., and Kirkegaard, K. (2002b). Similar structural basis for membrane localization and protein priming by an RNA-dependent RNA polymerase. J. Biol. Chem. *277*, 16324–16331.

McKnight, K.L., and Lemon, S.M. (1998). The rhinovirus type 14 genome contains an internally located RNA structure that is required for viral replication. RNA *4*, 1569–1584.

McRee, D.E. (1992). XtalView: a visual protein crystallographic system for X11/Xview. J. Mol. Graph. *10*, 44–47.

Merrit, E.A., and Bacon, D.J. (1997). Raster3D: photorealistic molecular graphics. Methods Enzymol. *277*, 505–524.

Ng, K.K.S., Cherney, M.M., Vazquez, A.L., Machnin, A., Alonso, J.M.M., Parra, F., and James, M.N.G. (2002). Crystal structures of active and inactive conformations of a caliciviral RNA-dependent RNA polymerase. J. Biol. Chem. *277*, 1381–1387.

O'Farrell, D., Trowbridge, R., Rowlands, D., and Jager, J. (2003). Substrate complexes of hepatitis C virus RNA polymerase (HC-J4): structural evidence for nucleotide import and de-novo initiation. J. Mol. Biol. *326*, 1025–1035.

Otwinowski, Z., and Minor, W. (1997). Processing X-ray diffraction data collected in oscillation mode. In Methods in Enzymology, C.W. Carter, Jr. and R.M. Sweet, eds. (New York: Academic Press), pp. 307–326.

Pata, J.D., Schultz, S.C., and Kirkegaard, K. (1995). Functional oligomerization of poliovirus RNA-dependent RNA polymerase. RNA *1*, 466–477.

Pathak, H.B., Ghosh, S.K., Roberts, A.W., Sharma, S.D., Yoder, J.D., Arnold, J.J., Gohara, D.W., Barton, D.J., Paul, A.V., and Cameron, C.E. (2002). Structure-function relationships of the RNA-dependent RNA polymerase from poliovirus (3Dpol). A surface of the primary oligomerization domain functions in capsid precursor processing and VPg uridylylation. J. Biol. Chem. *277*, 31551–31562.

Patick, A.K., Binford, S.L., Brothers, M.A., Jackson, R.L., Ford, C.E., Diem, M.D., Maldonado, F., Dragovich, P.S., Zhou, R., Prins, T.J., et al. (1999). In vitro antiviral activity of AG7088, a potent inhibitor of human rhinovirus 3C protease. Antimicrob. Agents Chemother. *43*, 2444–2450.

Paul, A.V., van Boom, J.H., Filippov, D., and Wimmer, E. (1998). Protein-primed RNA synthesis by purified poliovirus RNA polymerase. Nature *393*, 280–284.

Ponstingl, H., Henrick, K., and Thornton, J.M. (2000). Discriminating between homodimeric and monomeric proteins in the crystalline state. Proteins *41*, 47–57.

Racaniello, V.R. (2001). Picornaviridae: the viruses and their replication. In Fields Virology, D.M. Knipe and P.M. Howley, eds. (Philadelphia: Lippincott Williams & Wilkins), pp. 685–722.

Sali, A., and Blundell, T.L. (1993). Comparative protein modelling by satisfaction of spatial restraints. J. Mol. Biol. *234*, 779–815.

Skern, T., Sommergruber, W., Blaas, D., Gruendler, P., Fraundorfer, F., Pieler, C., Fogy, I., and Kuechler, E. (1985). Human rhinovirus 2: complete nucleotide sequence and proteolytic processing signals in the capsid protein region. Nucleic Acids Res. *13*, 2111–2126.

Steitz, T.A. (1999). DNA polymerases: structural diversity and common mechanisms. J. Biol. Chem. *274*, 17395–17398.

Toney, M.D., Hohenester, E., Cowan, S.W., and Jansonius, J.N. (1993). Dialkylglycine decarboxylase structure: bifunctional active site and alkali metal sites. Science *261*, 756–759.

Wang, M., Ng, K.K., Cherney, M.M., Chan, L., Yannopoulos, C.G., Bedard, J., Morin, N., Nguyen-Ba, N., Alaoui-Ismaili, M.H., Bethell, R.C., et al. (2003). Non-nucleoside analogue inhibitors bind to an allosteric site on HCV NS5B polymerase. Crystal structures and mechanism of inhibition. J. Biol. Chem. *278*, 9489–9495.

Accession Numbers

Atomic coordinates for HRV14/Sm^{3+}, HRV1B/K^{+}, and HRV16 $3D^{pol}$ have been deposited in the Protein Data Bank with access codes 1TEB, 1TE8, and 1TE9, respectively.